

# Quantum circuits for the Ising spin networks

Grzegorz Czelusta and Jakub Mielczarek\*

*Institute of Theoretical Physics, Jagiellonian University, Lojasiewicza 11, 30-348 Cracow, Poland*

(Dated: April 10, 2023)

Spin network states are a powerful tool for constructing the  $SU(2)$  gauge theories on a graph. In loop quantum gravity (LQG), they have yielded many promising predictions, although progress has been limited by the computational challenge of dealing with high-dimensional Hilbert spaces. To explore more general configurations, quantum computing methods can be applied by representing spin network states as quantum circuits. In this article, we introduce an improved method for constructing quantum circuits for 4-valent Ising spin networks, which utilizes a smaller number of qubits than previous approaches. This has practical implications for the implementation of quantum circuits. We also demonstrate the procedure with various examples, including the construction of a 10-node Ising spin network state. The key ingredient of the method is the variational transfer of partial states, which we illustrate through numerous examples. Our improved construction provides a promising avenue for further exploring the potential of quantum computing methods in quantum gravity research.

## I. INTRODUCTION

Quantum circuit representation of gravitational states is a crucial area of research for several reasons. Firstly, it provides a framework for quantum simulations of quantum gravitational processes. Secondly, it offers a powerful tool to investigate the holographic properties of gravitational interactions. Thirdly, the quantum circuit representation can provide an upper bound on the quantum complexity of gravitational processes. Overall, the development of quantum circuit representations of gravitational states has the potential to advance our understanding of fundamental physics and also contribute to the development of quantum technologies.

In this study, we address the issue of the quantum circuit representation of the Ising spin network states within the context of loop quantum gravity (LQG) [1, 2]. These states offer an intermediary level of complexity between the symmetry-reduced and general configurations, making them a valuable tool for investigating quantum collective phenomena in the realm of quantum gravity.

The Ising spin network states [3] are represented by graphs built out of the 4-valent nodes only. Furthermore, the links (holonomies) are associated with the fundamental ( $j = 1/2$ ) representations of the  $SU(2)$  group. In consequence, at the nodes, four spin-1/2 Hilbert spaces  $\mathcal{H}_{\frac{1}{2}}$ , associated with the holonomies, meet.

The invariance with respect to the local gauge symmetry (imposed by the Gauss law) implies that the states  $|\mathcal{I}\rangle$  at the nodes are spanned by the invariant, so-called *intertwiner*, spaces:

$$|\mathcal{I}\rangle \in \text{Inv}_{SU(2)} \left( \mathcal{H}_{\frac{1}{2}} \otimes \mathcal{H}_{\frac{1}{2}} \otimes \mathcal{H}_{\frac{1}{2}} \otimes \mathcal{H}_{\frac{1}{2}} \right). \quad (1)$$

Here, the invariant Hilbert space is two-dimension, justifying the reason for using the Ising spin network terminology.

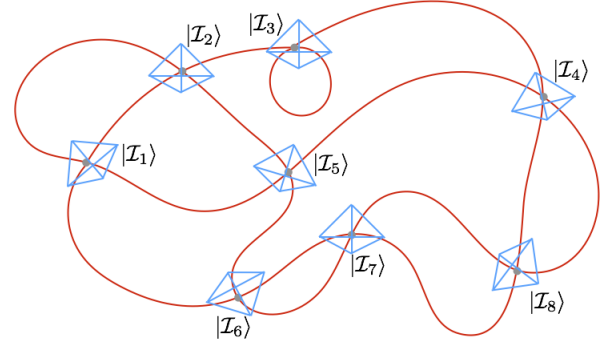


FIG. 1. An exemplary Ising spin network with tetrahedra being dual to the 4-valent nodes.

The general state of a spin network can be represented as a product of intertwiner states at each node, i.e.,  $\otimes_n |\mathcal{I}_n\rangle$ . However, it is also possible to consider a superposition of spin network base states, especially when the spin networks are constructed using entanglement carried by the holonomies. Such a state would be a superposition of different spin network states. However, the Gauss constraint can be used to project the state onto a particular spin network state. Thus, while a general spin network state can be represented as a product of intertwiner states, it can also be described as a superposition of spin network base states, which can be projected onto a specific spin network state by enforcing the Gauss constraint.

Within LQG, the geometric operators (e.g., area or volume) have a clear geometric interpretation in terms of the spin network states. Specifically, 4-valent nodes are associated with non-zero quanta of volume, and the links describe their relative adjacency. For Ising spin networks, the nodes are dual to tetrahedra, as depicted in Fig. 1. The links, or holonomies, encode the adjacency of the faces of the tetrahedra.

The application of quantum computing methods to

\* jakub.mielczarek@uj.edu.pl

simulate spin networks was first explored in Ref. [4]. In this article, the Ising spin network was considered, allowing for the introduction of the notion of qubits. The model was implemented on a molecular NMR quantum simulator, enabling some initial quantum computations to be performed, specifically in the context of spin foam vertex amplitudes. Shortly after, another article on a similar subject was released [5], which used the same concept of the “intertwiner qubit”. However, these studies were not conducted in the context of universal quantum computing, but instead focused on adiabatic quantum computers (quantum annealers). Overall, these pioneering works pave the way for future developments in the field.

Ref. [6] represents a further advancement in the study of quantum simulations of spin networks in LQG. This article describes the first-ever quantum simulations of nodes in the spin network using a superconducting quantum processor. A five-qubit superconducting quantum chip provided by IBM’s cloud services has been used for this purpose. In addition, a method for evaluating transition amplitudes and the spin foam vertex amplitudes have been developed. Building on this work, Ref. [7] introduces a quantum circuit that enables the preparation of a general intertwiner qubit state of the Ising spin network node.

Ref. [8] proposes the use of photonic circuits to simulate spin foam amplitudes, which employs the intertwiner qubits introduced previously. This approach offers several advantages, including its applicability to spin-foam amplitudes with spin labels  $j \gg 1/2$ , which is difficult to determine using classical computations [9, 10]. Recently, Ref. [11] reported the first experimental demonstration of the photonic approach applied to evaluating the spin-foam vertex amplitude.

In Ref. [12], a significant step towards more advanced simulations of spin foam amplitudes was taken using a 10-qubit superconducting quantum processor. This marks the most sophisticated simulation of this kind to date. The implementation of intertwiner qubits directly allowed for the achievement of results, with only a single logical qubit needed to encode a node of a spin network and five for computing a spin foam vertex amplitude in Ooguri’s model [13]. However, the construction of relevant states is not straightforward and requires the application of optimization techniques. Nonetheless, the approach shows promise since it can potentially simulate spin networks with four times more nodes with the same quantum computing resources. Additionally, this approach has the potential to extend beyond the  $j = 1/2$  case, making it an exciting avenue for further exploration.

In this article, we present a novel extension of existing methods to the case of spin networks with an arbitrary number of nodes and an arbitrary network structure, although we limit our analysis to 4-valent nodes and links with  $1/2$  spins. Specifically, we focus on spin networks corresponding to *vector geometries* [14], although our method can be easily extended to other types of net-

works. Our main objective is to develop a methodology to represent any Ising spin network as a quantum circuit, to be executed on a quantum processor, and to measure relevant physical quantities.

This article is organized as follows. In Section II, we introduce a new quantum circuit for the node of the Ising spin network, which will play a crucial role in the overall procedure described in this article. In Section III, we discuss the general procedure for constructing a spin network from entangled states of the links. Drawing on the results of the previous sections, we propose a new projection scheme in Section IV and illustrate it using the example of the dipole spin network. Section V describes the variational technique used to transfer the spin network states onto an ansatz circuit, which is crucial for our optimized method of constructing quantum circuits for arbitrary Ising spin networks. The method is presented in Section VI, where numerous examples can also be found. Finally, in Section VII, we provide further details of the computations, including the use of quantum hardware. We summarize our results and suggest further research directions in the discussed area in Section VIII.

## II. A SINGLE NODE CIRCUIT

In our previous article [7], we presented a quantum circuit that can create an arbitrary state for a single node in the Ising spin network. This state can be expressed in the following form:

$$\begin{aligned} |\mathcal{I}\rangle &= \cos(\theta/2)|\iota_0\rangle + e^{i\phi} \sin(\theta/2)|\iota_1\rangle \\ &= \frac{c_1}{\sqrt{2}}(|0011\rangle + |1100\rangle) \\ &\quad + \frac{c_2}{\sqrt{2}}(|0101\rangle + |1010\rangle) \\ &\quad + \frac{c_3}{\sqrt{2}}(|0110\rangle + |1001\rangle), \end{aligned} \quad (2)$$

where  $\theta$  and  $\phi$  are angles on the Bloch sphere and  $\{|\iota_0\rangle, |\iota_1\rangle\}$  form an orthonormal basis of the invariant subspace. The coefficients  $c_1$ ,  $c_2$  and  $c_3$  are certain functions of  $\theta$  and  $\phi$  (see Ref. [7] for details), satisfying the two conditions:

$$\sum_{i=1}^3 |c_i|^2 = 1, \quad \text{and} \quad \sum_{i=1}^3 c_i = 0. \quad (3)$$

In Ref. [7], a quantum circuit is proposed to generate the state (2). The circuit’s structure is depicted in Fig. 2.

Here, the gates  $V$  and  $U$  are given by the following unitary matrices:

$$V = \begin{pmatrix} -\frac{c_2}{\sqrt{|c_2|^2 + |c_3|^2}} & \frac{c_3^*}{\sqrt{|c_2|^2 + |c_3|^2}} \\ -\frac{c_3}{\sqrt{|c_2|^2 + |c_3|^2}} & -\frac{c_2^*}{\sqrt{|c_2|^2 + |c_3|^2}} \end{pmatrix}, \quad (4)$$

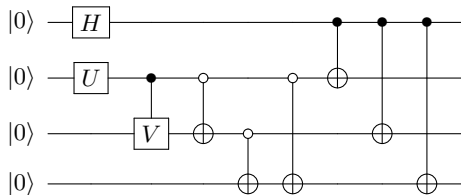


FIG. 2. A quantum circuit generating a state of a single node of the Ising spin network, introduced in Ref. [7].

$$U = \begin{pmatrix} c_1 & \sqrt{|c_2|^2 + |c_3|^2} \\ -\sqrt{|c_2|^2 + |c_3|^2} & c_1^* \end{pmatrix}. \quad (5)$$

A new version of the circuit is proposed in this article, which involves defining the operator  $\hat{W}$ . This operator can transform a single-qubit state ( $\alpha|0\rangle + \beta|1\rangle$ ) into the four-qubit intertwiner state.

$$\hat{W}(\alpha|0\rangle + \beta|1\rangle)|000\rangle = |\mathcal{I}(\alpha, \beta)\rangle = \alpha|\iota_0\rangle + \beta|\iota_1\rangle. \quad (6)$$

The construction is made such that the coefficients  $\alpha$  and  $\beta$  of the single-qubit state (in the  $\{|0\rangle, |1\rangle\}$  basis) map one-to-one onto the coefficients of the intertwiner qubit in the  $\{|\iota_0\rangle, |\iota_1\rangle\}$  basis. Therefore, in order to obtain an intertwiner state represented on 4 qubits, we need to create the corresponding 1-qubit state and subsequently apply the operator  $\hat{W}$ . The property will play an essential role in our further considerations.

The quantum circuit representation of the Eq. 6 is shown in Fig. 3. In the definition of the operator  $\hat{W}$ , one applies the rotation operator  $R_y(\theta)$ , where the rotation angle is fixed to be  $\theta = 2 \arccos \frac{1}{\sqrt{3}}$ . Furthermore, the square root of the *SWAP* gate has the following matrix representation:

$$\sqrt{SWAP} = \begin{pmatrix} 1 & 0 & 0 & 0 \\ 0 & \frac{1+i}{2} & \frac{1-i}{2} & 0 \\ 0 & \frac{1-i}{2} & \frac{1+i}{2} & 0 \\ 0 & 0 & 0 & 1 \end{pmatrix}. \quad (7)$$

In the Appendix, one can find an explicit circuit for the  $\sqrt{SWAP}$  gate. This circuit is expressed in terms of elementary single- and two-qubit gates, which makes it useful for practical implementations. Furthermore, the Appendix provides an alternative circuit for the  $\hat{W}$  circuit, with employed variational ansatz.

### III. GLUING TETRAHEDRA

Spin network states can be constructed by first defining the states of the links, and then projecting each node onto the intertwiner basis states. We can denote the state of a link  $l$  as  $|\alpha^{(l)}\rangle$ . With this notation, the spin network state can be expressed as follows:

$$|\Gamma, \alpha_l\rangle = \hat{P}_\Gamma \bigotimes_l |\alpha_l\rangle, \quad (8)$$

where  $\hat{P}_\Gamma$  is the projection operator (satisfying  $\hat{P}_\Gamma^2 = \hat{P}_\Gamma$ ), associated with the Gauss constraint, which can be expressed as follows:

$$\hat{P}_\Gamma := \sum_{j_l, \mathcal{I}_n} |\Gamma, j_l, \mathcal{I}_n\rangle \langle \Gamma, j_l, \mathcal{I}_n|. \quad (9)$$

The classical phase-space structure that arises from spin networks is called twisted geometry [15]. A typical configuration of this geometry corresponds to a collection of uncorrelated tetrahedra (or, in the case of networks with higher valency, polyhedra). This uncorrelated structure of the twisted geometry is reflected by the uncorrelated structure of the spin network basis states:

$$|\Gamma, j_l, \mathcal{I}_n\rangle = \bigotimes_n |\mathcal{I}_n\rangle, \quad (10)$$

which is a product state, not exhibiting entanglement between the nodes.

In this article, we will focus on vector geometries, which have a more rigid structure compared to other geometries. Specifically, in vector geometries, the normals to adjacent faces in neighboring tetrahedra are oriented back-to-back. Despite this specific focus, it is important to note that the method presented in this article is completely general and applicable to arbitrary types of links.

It has been justified in Ref. [16] that the vector geometry can be obtained by using the squeezed states on the links:

$$|\mathcal{B}, \lambda_l\rangle = \left(1 - |\lambda_l|^2\right) \sum_j \sqrt{2j+1} \lambda_l^{2j} |\mathcal{B}, j\rangle, \quad (11)$$

where  $\lambda_l \in \mathbb{C}$  is a free parameter of the state. The  $|\mathcal{B}, j\rangle$  is a singlet state of spin  $j$ , which is maximally entangled

$$|\mathcal{B}, j\rangle = \frac{1}{\sqrt{2j+1}} \sum_{m=-j}^j (-1)^{j-m} |j, m\rangle_s |j, -m\rangle_t. \quad (12)$$

Subsequently, projection on a spin-network basis states is performed, leading to:

$$|\Gamma, \mathcal{B}, \lambda_l\rangle = \hat{P}_\Gamma \bigotimes_l |\mathcal{B}, \lambda_l\rangle. \quad (13)$$

Specifically, for the case of the Ising spin networks ( $j = 1/2$ ) we obtain:

$$|\mathcal{B}, j\rangle = \frac{1}{\sqrt{2}} \left( \left| \frac{1}{2}, \frac{1}{2} \right\rangle \left| \frac{1}{2}, -\frac{1}{2} \right\rangle - \left| \frac{1}{2}, -\frac{1}{2} \right\rangle \left| \frac{1}{2}, \frac{1}{2} \right\rangle \right) \quad (14)$$

or, equivalently, in the qubit notation:

$$\left| \mathcal{B}, \frac{1}{2} \right\rangle = \frac{1}{\sqrt{2}} (|01\rangle - |10\rangle). \quad (15)$$

Previous studies have focused on spin networks constructed from the singlet state 15. In particular, Refs.

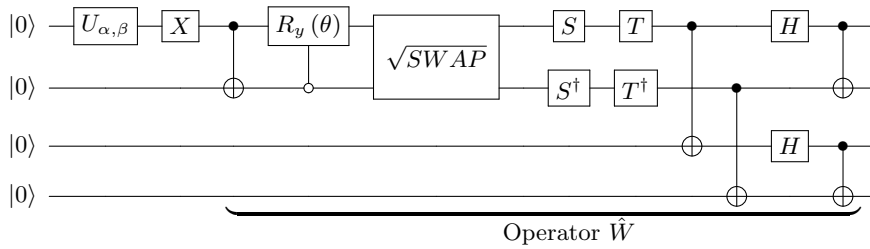


FIG. 3. Quantum circuit for the operator  $\hat{W}$  which turns the state  $(\alpha|0\rangle + \beta|1\rangle)|000\rangle$  to  $|\mathcal{I}(\alpha, \beta)\rangle = \alpha|\iota_0\rangle + \beta|\iota_1\rangle$ . Here, the gate  $\hat{U}_{\alpha, \beta}$  acts as follows:  $\hat{U}|0\rangle = \alpha|0\rangle + \beta|1\rangle$ . The rotation angle of the rotation gate  $R_y(\theta)$  is fixed to be  $\theta = 2 \arccos \frac{1}{\sqrt{3}}$ . The  $\sqrt{SWAP}$  is a squared SWAP gate, the matrix representation of which is given in Eq. 7. Furthermore,  $S = \sqrt{Z}$  and  $T = \sqrt[4]{Z}$ , where  $Z$  denotes Pauli  $Z$  gate,  $X$  is the Pauli  $X$  gate and  $H$  is the Hadamard gate.

[4, 7] conducted quantum simulations of simple spin networks (dipole and pentagram) using this singlet state. Notably, it has been observed that the states of these spin networks correspond to the PEPS tensor networks [7] implying the area law for entanglement entropy [17–19].

One potential drawback of this approach is that the number of qubits involved in the computation can quickly become quite large. Specifically, since each link in the Ising spin network state corresponds to a 2-qubit state, a network with  $l$  links requires  $2l$  qubits to be initially involved. For example, the pentagram spin network has  $l = 10$ , which means that 20 qubits are required initially. While applying the Gauss projection at the nodes can reduce the Hilbert space to just 5 intertwiner qubits, this still means that the majority of the initial quantum resources are not used by the final state. This inefficiency becomes even more pronounced when dealing with more complicated spin networks.

To address this issue, a method for constructing Ising spin networks that uses far fewer quantum resources is needed. In the subsequent sections, we propose a concrete procedure for achieving this goal.

#### IV. PROJECTION ONTO THE INTERTWINER SUBSPACE

This section outlines the initial stage of constructing Ising spin networks, which involves reducing the number of qubits required for the process.

For this purpose, let us consider the states of the links, in accordance with the discussion presented in the previous section. For the Bell states (15) of the links, the corresponding quantum circuit, employing elementary gates, is shown in Fig. 4.

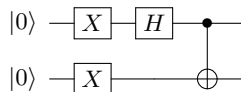


FIG. 4. Quantum circuit for the Bell state (15).

In our previous studies in Refs. [6, 7], the states of the

links were projected onto the spin network basis states, generated by the sequence of the quantum circuits shown in Fig. 2. In this way the quantum amplitudes of the entangled links in the spin network basis were reconstructed. However, the approach does not lead to the final state directly.

Here, we observe that the  $\hat{W}$  operator, introduced in Fig. 3, can be used to define projection operator, equipped with the mapping onto a single-qubit state. For this purpose, we apply  $\hat{W}^\dagger$  and then project some of the qubits (see Fig. 5) onto the  $|0\rangle$  states.

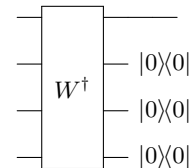


FIG. 5. Projection operator on the intertwiner subspace, expressed in one-qubit representation.

To achieve the desired projection, measurements are conducted, and only those returning  $|0\rangle$  for the last three qubits are accepted. In the chosen outcomes, the first qubit stores the intertwiner state.

Although vector geometries are utilized in this work, the proposed method can be adapted to other types of spin networks. To achieve this, alternative states, rather than Bell pairs, must be prepared and subsequently projected. Notably, the operator  $\hat{W}$  described in this study is specific to Ising spin networks. Nevertheless, its extension to higher dimensions of the intertwiner space is likely feasible.

#### A. Dipole

To demonstrate the newly introduced projection technique, we analyze its application to the dipole spin network, which is presented in Fig. 6.

As shown in Fig. 7, using the maximally entangled pairs  $|\mathcal{B}, \frac{1}{2}\rangle$  (generated by the circuit shown in Fig. 4), the states of the links are created first. Then the projection operator (generated by the circuit shown in Fig.

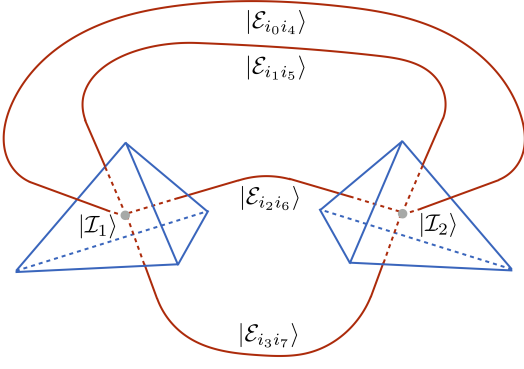
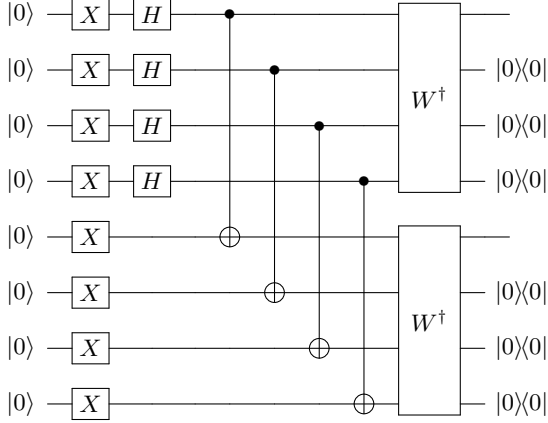


FIG. 6. The dipole spin network.

5) is applied for the two nodes. The unmeasured qubits (0th and 4th from the top) carry the state of the dipole spin network.

FIG. 7. Quantum circuit representing projection of state  $\bigotimes_{l \in \Gamma_2} |\mathcal{B}, \frac{1}{2}\rangle$ .

By conducting quantum tomography on the 0th and 4th qubits and discarding any measurement results with non-zero values on qubits 1, 2, 3, 5, 6, and 7, we can extract the dipole state. This method enables us to obtain the density matrix of the dipole state, which comprises only two logical qubits, as anticipated for the two intertwiner qubits of the Ising dipole spin network.

On the other hand, the dipole state can easily be computed by the following contraction of the Wigner  $4j$ -symbols  $\iota_k^{m_1 m_2 m_3 m_4}$ :

$$\begin{aligned} |\Gamma_2, \mathcal{B}, \frac{1}{2}\rangle &= \hat{F}_\Gamma \bigotimes_{l \in \Gamma_2} |\mathcal{B}, \frac{1}{2}\rangle \\ &= \sum_{k,l} \iota_{(k)}^{m_1 m_2 m_3 m_4} \iota_{(l) m_1 m_2 m_3 m_4} |\iota_k \iota_l\rangle \\ &= \frac{1}{\sqrt{2}} (|\iota_0 \iota_0\rangle + |\iota_1 \iota_1\rangle). \end{aligned} \quad (16)$$

Furthermore, the  $4j$ -symbols can be expressed in terms

of the  $3j$ -symbols:

$$\begin{aligned} \iota_k^{m_1 m_2 m_3 m_4} &= \sqrt{2k+1} \begin{pmatrix} m_1 & m_2 & m \\ j_1 & j_2 & k \end{pmatrix} \\ &\cdot g_{mm'} \begin{pmatrix} m' & m_3 & m_4 \\ k & j_3 & j_4 \end{pmatrix} \end{aligned} \quad (17)$$

where

$$g_{mm'} = \delta_{m,-m'} (-1)^{j-m}. \quad (18)$$

The indices of Wigner  $4j$ -symbols can be lowered and raised using the  $g_{mm'}$  tensor.

As observed, the dipole spin network's final state can be encoded using only two of the original eight qubits utilized in its construction. Although the final 2-qubit state can be reconstructed using quantum tomography, it is essential to find its reduced circuit representation afterward. To avoid the need for quantum tomography, we present a variational method in the following section to construct the circuit.

## V. VARIATIONAL TRANSFERRING OF QUANTUM STATE

Quantum circuit for some unknown state can be approximated (or even given exactly) by employing a quantum circuit ansatz. In particular, the projected state of the spin network can be transferred into an ansatz circuit, without knowing the explicit form of the state, by fixing the parameters of the circuit. The obtained circuit is characterised by smaller number of qubits that the original (unprojected) state, which is convenient for the quantum computing purposes.

Here, we use the so-called Simplified-Two-Design ansatz, which consists of layers of Pauli-Y rotations and controlled-Z entanglers proposed in Ref. [20]. The quantum circuit for the ansatz is shown in Fig. 8, for the case with 5 qubits.

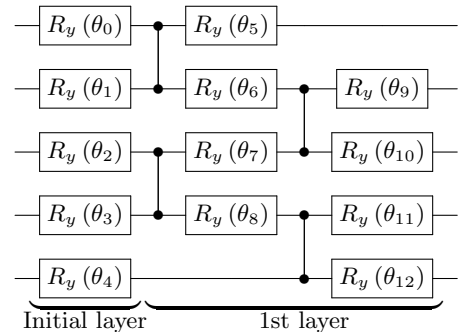


FIG. 8. Quantum circuit for the simplified-two-design ansatz with one layer.

In what follows, fidelities are used to quantify the quantum states generated by the ansatz circuits. Both the

classical fidelity:

$$F(p, q) := \sum_i \sqrt{p_i q_i}, \quad (19)$$

where  $p$  and  $q$  are probabilities of basis states, and the quantum fidelity:

$$F(\hat{\rho}_1, \hat{\rho}_2) := \left( \text{tr} \sqrt{\sqrt{\hat{\rho}_1} \hat{\rho}_2 \sqrt{\hat{\rho}_1}} \right)^2, \quad (20)$$

where  $\hat{\rho}_1$  and  $\hat{\rho}_2$  are density matrices of two states will be used.

### A. Dipole

Applying the quantum circuit shown in Fig. 7, the resulting 0th and 4th qubit state can be projected onto the ansatz circuit shown in Fig. 8. This results in the quantum circuit presented in Fig. 9, which allows transferring the dipole state.

The transfer is performed variationally by minimizing the following cost function:

$$\text{cost}(\vec{\theta}) = 1 - \text{Prob}(q_0 q_4 = 00), \quad (21)$$

where the parameter vector  $\vec{\theta} = (\theta_1, \theta_2, \theta_3, \theta_4)$ , contains the four angles to be fixed. We use classical optimizers, gradient descent optimizers, and Adam optimizers. Technical details and parameters can be found in our GitHub repository [21].

By taking the conjugation of the ansatz with the parameters obtained from minimizing the cost function, we can prepare the dipole state using the quantum circuit depicted in Fig.10. This circuit is designed to transform the initial state into the desired dipole state, utilizing the parameters obtained from the optimization process.

The transferred dipole circuit (Fig. 10) has been thereafter executed on the superconducting Manila IBM quantum processor, resulting in the fidelities shown in Tab. I.

	without correction	with correction
classical	0.96	0.9968
quantum	0.89	0.99

TABLE I. Fidelities for dipole spin network.

In our work, we utilized measurement error mitigation as a means of correction. For the dipole state, the proposed ansatz can accurately express the state, leading to a fidelity that can be made arbitrarily close to 1. To delve into the technical details and results of our research, as well as the opportunity to experiment with our simulations, please refer to our GitHub repository [21].

The table with the found parameters of the ansatz for the dipole is presented in Tab. II.

-1.06	3.65
4.72	1.57

TABLE II. Determined parameters for dipole ansatz. The structure of the table corresponds to the structure of ansatz Fig. 8, with one layer.

### B. Pentagon

In the case of the pentagram spin network shown in Fig. 24 the projected state has the form:

$$\hat{P}_\Gamma |\psi\rangle = \sum_{\iota_{k_i}} \overline{\{15j\}} |\iota_{k_1} \iota_{k_2} \iota_{k_3} \iota_{k_4} \iota_{k_5}\rangle, \quad (22)$$

where the  $15j$  symbol can be expressed in terms of the  $4j$  symbols as follows:

$$\{15j\} = \iota_1^{m_{12} m_{13} m_{14} m_{15}} \iota_{2; m_{12}}^{m_{13} m_{14} m_{15}} \iota_{3; m_{12} m_{13}}^{m_{14} m_{15}} \iota_{4; m_{12} m_{13} m_{14}}^{m_{15}} \iota_{5; m_{12} m_{13} m_{14} m_{15}}. \quad (23)$$

For the Ising spin network case, the state can be obtained using the quantum circuits presented in Fig. 12.

Here, the state  $|\psi\rangle = \hat{U}_\psi |0\rangle^{\otimes 20} = \bigotimes_{\iota \in \Gamma_5} |\mathcal{B}, \frac{1}{2}\rangle$  is a product of the singlet pairs, i.e. multiple time use of the circuit shown in Fig. 4. Employing similar techniques as in the case of a dipole, we can transfer the pentagram state on the ansatz of the type shown in Fig. 8, with 3 layers.

Ansatz for the pentagram state with four layers and five qubits is shown in Fig. 8. The explicit form of the ansatz and the found parameters can be found at the GitHub repository [21].

In order to emphasize the complexity of the quantum circuit for the variational transfer of the pentagram Ising spin network state, we show its explicit form in Fig. 13.

The obtained ansatz has been executed on the IBM quantum computer Manila and the measured fidelities are shown in Tab. III.

	without correction	with correction
classical	0.87	0.93
quantum	0.6	0.77

TABLE III. Fidelities for the pentagram spin network.

The determined parameters of the ansatz for the pentagram are shown in Tab. V.

## VI. GLUING NETWORKS

Generating the Ising spin networks in the way presented so far requires the number of qubits to be four times greater than the number of nodes. This is becoming problematic while attempting to simulate higher valence spin networks, which are relevant e.g. to study

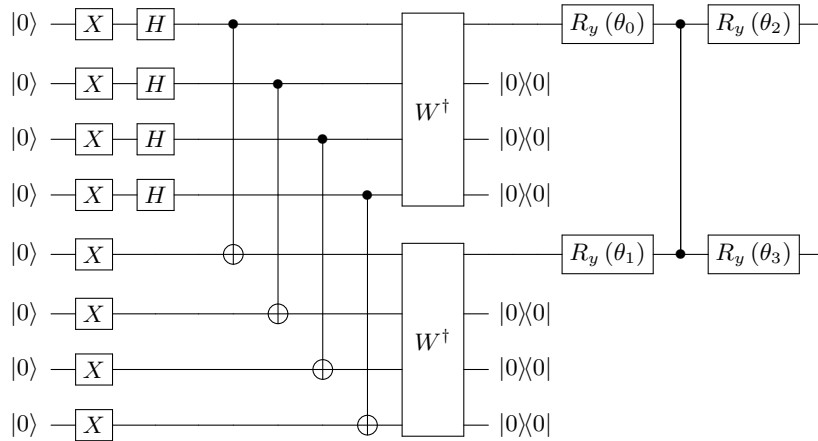


FIG. 9. Projection of state  $\bigotimes_{l \in \Gamma_2} |\mathcal{B}, \frac{1}{2}\rangle$  and transferring on simplified-two-design two-qubits ansatz.

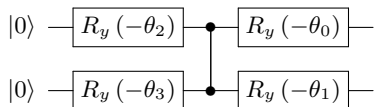


FIG. 10. Transferred projection of the state  $\bigotimes_{l \in \Gamma_2} |\mathcal{B}, \frac{1}{2}\rangle$ , i.e. adjoint ansatz.

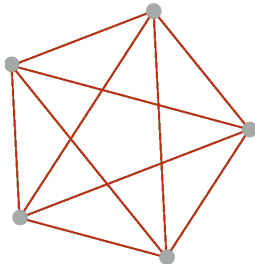


FIG. 11. The pentagram spin network.

3.51	1.88		1.21		2.29	
3.80	0.77	1.09	-0.15	4.99	4.96	4.78
0.33	2.35	1.27	2.69	1.73	0.82	1.08
5.04	0.02	4.82	4.90	4.65	6.10	1.96
3.43		3.33		4.26		5.48

TABLE IV. Found parameters for pentagram ansatz. The structure of the table corresponds to the structure of ansatz Fig. 8, with three layers.

collective properties in quantum gravity. However, as we have shown in the previous section, states of the Ising spin networks can eventually be transferred to the quantum circuit employing the number of logical qubits equal to the number of nodes.

Here we propose an approach for constructing large Ising spin networks by utilizing smaller, pre-existing *open* spin networks. This method involves transferring the quantum states in advance to reduce the number of qubits needed. To achieve this, we consider a “brick”

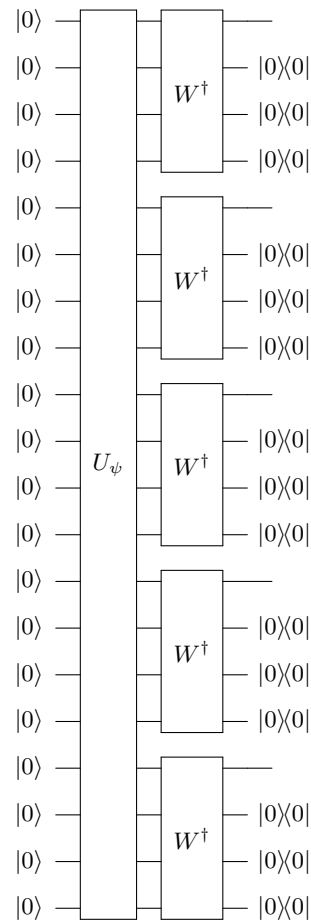


FIG. 12. Quantum circuit representing projection of the state  $|\psi\rangle = \bigotimes_{l \in \Gamma_5} |\mathcal{B}, \frac{1}{2}\rangle$ .

spin network with certain links left open, allowing for further connections to be made. For instance, in the case of the pentagram spin network, we can obtain the corresponding “brick” spin network by removing one of the nodes and leaving the four adjacent links open, as de-

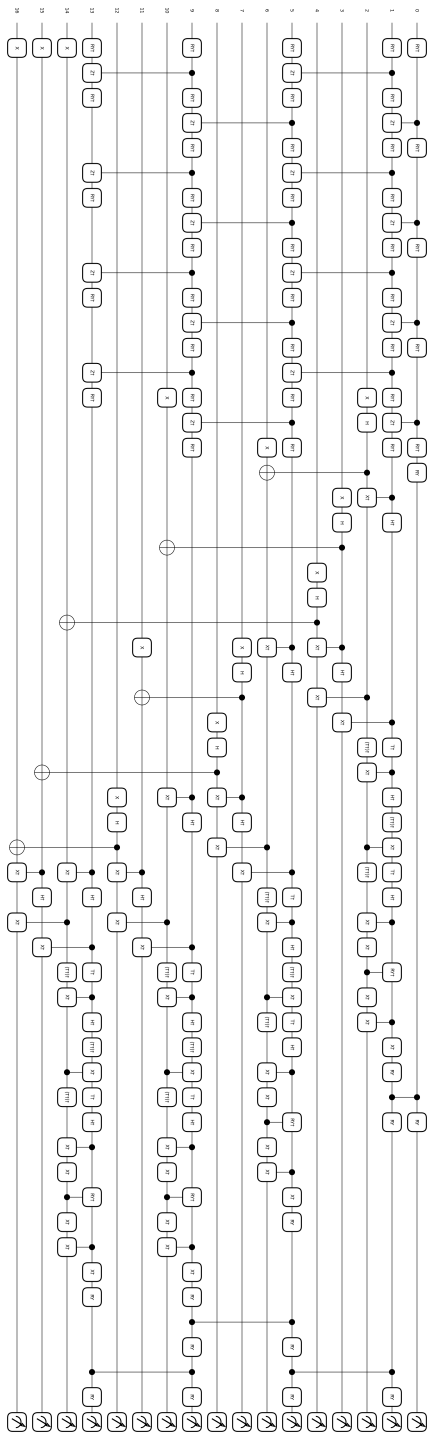


FIG. 13. Quantum circuit used for the variational transfer of the pentagram Ising-type spin network state (see from the left side).

picted in Fig. 14. By utilizing this technique, we can construct large-scale Ising spin networks more efficiently and with fewer qubits than previously possible.

It must be emphasized that our definition of an open spin network is a little different than some other used in

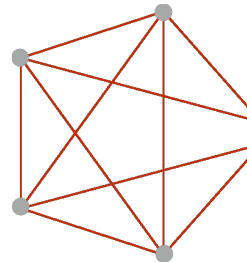


FIG. 14. A brick-type pentagram network with four open links.

the literature [22]. For example, in the case of an open single node, its state is equal to the state of a dipole with only one projection, i.e. contraction of four spin pairs with one intertwiner:

$$l_k^{m_{12}m_{13}m_{14}m_{15}} \alpha_{m_{12}m_2} \alpha_{m_{13}m_3} \alpha_{m_{14}m_4} \alpha_{m_{15}m_5}, \quad (24)$$

where one spin from each pair (which is not contracted within the intertwiner) forms a boundary. So, in the definition applied here, boundary spins live at the ends of free links. Following the other definition it would be just that the intertwiner forming the boundary, *i.e.*:

$$l_k^{m_{12}m_{13}m_{14}m_{15}}. \quad (25)$$

So, in other definition, the boundary is defined at the open node, which is not connected to other nodes.

The quantum circuit corresponding to the brick-type (open) pentagram spin network is shown in Fig. 15.

The pentagram spin network, with one removed node, can be accurately represented by an ansatz that utilizes only 8 qubits. This is a significant reduction compared to the unprojected case, which requires 20 qubits. In general, an  $n$ -node Ising spin network with one removed node can be represented by  $n + 3$  qubits. By connecting two networks, one with  $n$  nodes and the other with  $m$  nodes, we can obtain a network with  $n + m$  nodes using  $n + m + 6$  qubits. In contrast, constructing the same network from individual singlet pairs would require  $4(n + m)$  qubits. This represents a significant saving of quantum resources, with the amount saved being  $3(n + m) - 6$ , particularly for larger networks. Importantly, this procedure can be iteratively applied to construct arbitrarily large networks by attaching the basis brick-type spin networks in succession. To illustrate this procedure, we provide an example using a 10-node spin network.

The use of partially projected states to construct a larger Ising spin network is possible because the projectors act on different nodes and therefore commute. For the case of a 10-node Ising spin network we can prepare 20 links and then, apply 10 projections at once, or prepare, twice, 10 links for the pentagram, there apply four projections, and then apply the last two projections dur-



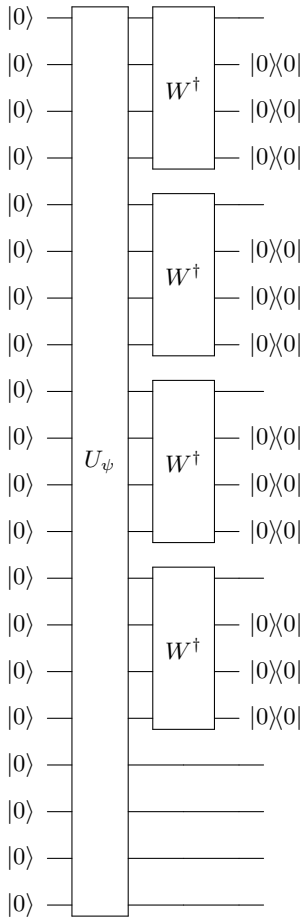


FIG. 15. Partially projected state  $|\psi\rangle = \bigotimes_{l \in \Gamma_5} |\mathcal{B}, \frac{1}{2}\rangle$ , i.e. pentagram with one open node

ing the gluing:

$$\begin{aligned} \hat{P}_\Gamma^{10\otimes} &= \hat{\mathbb{I}}^{4\otimes} \otimes \hat{P}_\Gamma^{2\otimes} \otimes \hat{\mathbb{I}}^{4\otimes} \cdot \left[ \left( \hat{P}_\Gamma^{4\otimes} \otimes \hat{\mathbb{I}} \right) \otimes \left( \hat{P}_\Gamma^{4\otimes} \otimes \hat{\mathbb{I}} \right) \right] \\ &= \left[ \left( \hat{P}_\Gamma^{4\otimes} \otimes \hat{\mathbb{I}} \right) \otimes \left( \hat{P}_\Gamma^{4\otimes} \otimes \hat{\mathbb{I}} \right) \right] \cdot \hat{\mathbb{I}}^{4\otimes} \otimes \hat{P}_\Gamma^{2\otimes} \otimes \hat{\mathbb{I}}^{4\otimes}. \end{aligned} \quad (26)$$

#### A. Gluing two pentagrams into a 10-node Ising spin network

Constructing a 10-node Ising spin network directly from the singlets at the links would require 40 logical qubits. This is already at the edge of the current capabilities of NISQ-type quantum technologies. However, by using the partial projection technique and gluing two brick-type pentagrams, we can generate the 10-node Ising spin network using only 16 qubits (8 qubits for each open pentagram). The procedure is illustrated in Fig. 16. This significantly reduces the quantum resources required for constructing larger spin networks and makes it feasible with current quantum technologies.

The quantum circuit associated with the gluing of two open pentagrams into the 10-node network is shown in

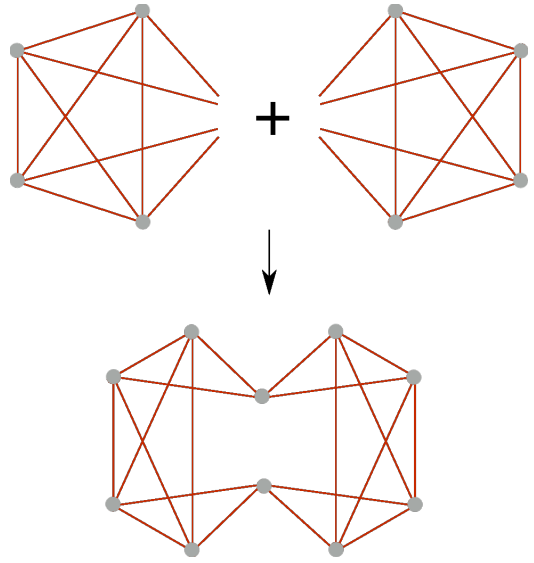


FIG. 16. A 10-node spin network obtained by gluing two open pentagrams.

Fig. 17.

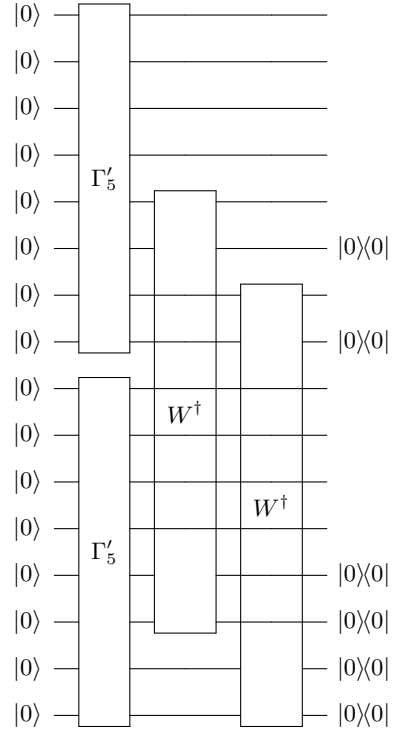


FIG. 17. Quantum circuit for gluing two open pentagrams.

In the case of the 10-node Ising spin network, Fig. 16, the projected state has the form:

$$\hat{P}_\Gamma |\psi\rangle = \sum_{l_{k_i}} c_{l_{k_1} l_{k_2} l_{k_3} l_{k_4} l_{k_5}} |l_{k_1} l_{k_2} l_{k_3} l_{k_4} l_{k_5}\rangle, \quad (27)$$

where

$$c_{\ell_k1\ell_k2\ell_k3\ell_k4\ell_k5} = \frac{m_{12}m_{13}m_{14}m_{15}}{\ell_1} \frac{m_{23}m_{24}m_{25}}{\ell_2} \frac{m_{34}m_{35}}{\ell_3} \frac{m_{45}}{\ell_4} \frac{m_{67}m_{68}m_{69}m_{610}}{\ell_7} \frac{m_{78}m_{79}m_{710}}{\ell_8} \frac{m_{89}m_{810}}{\ell_9} \frac{m_{910}}{\ell_{10}}. \quad (28)$$

The ansatz for the 10-node Ising spin network state is shown Fig. 8, which has 5 layers and 10 qubits.

2.52	2.15		0.11		0.78		2.86		1.75	
3.39	1.32	6.21	1.27	5.38	3.26	6.54	4.78	-0.19	0.04	5.21
1.28	4.34	4.11	6.43	1.81	0.24	1.59	2.04	3.74	2.02	4.37
4.76	2.00	6.28	3.14	1.20	0.83	-0.13	3.88	2.50	3.13	0.60
5.65	4.71	3.14	3.14	5.34	3.14	4.72	1.57	6.28	1.57	1.78
3.14	3.14	6.28	0.00	4.62	4.80	3.21	1.57	6.28	0.97	4.92
0.27	5.03	5.92	3.80	5.89	1.71	0.57	0.73	-0.02	2.21	4.57
5.64	5.07	1.78	1.68	1.39	5.72	5.20	3.37	5.95	-0.36	6.70
-0.31	5.73	2.36	5.08	3.53	0.81	0.84	3.07	1.44	5.06	0.33
4.08	3.35		1.32		2.12		0.68		4.56	

TABLE V. The parameters found for the 10-node network ansatz. The structure of table corresponds to structure of ansatz Fig. 8, with 5 layers and 10 qubits.

The fidelity between the states obtained from the quantum algorithm running on the classical simulator without noise and the states obtained from Eq. 28 is approximately 0.9975. It is reasonable to assume that the fidelity is essentially 1, up to numerical errors.

### B. Gluing single nodes into an arbitrary network

Another possibility in construction of the Ising spin networks is to prepare an ansatz circuit of a single node with four open links, depicted Fig. 18.

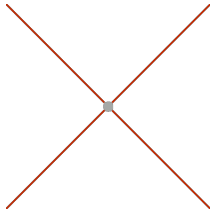


FIG. 18. One node with four open links.

The corresponding state can be expressed as follows:

$$|\Gamma'_2\rangle = \sum_{\ell_k} \ell_k^{m_{12}m_{13}m_{14}m_{15}} \alpha_{m_{12}m_2} \alpha_{m_{13}m_3} \alpha_{m_{14}m_4} \alpha_{m_{15}m_5} |\ell_k\rangle \left| \frac{1}{2}, m_2 \right\rangle \left| \frac{1}{2}, m_3 \right\rangle \left| \frac{1}{2}, m_4 \right\rangle \left| \frac{1}{2}, m_5 \right\rangle. \quad (29)$$

Based on the 8-qubit circuit shown in Fig. 19 the 5-qubit ansatz circuit can be constructed, which saves 3 qubits with respect to the original approach.

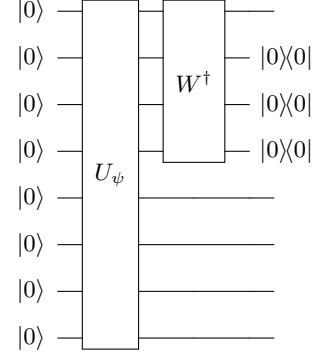


FIG. 19. Quantum circuit of a single node with four open links.

Gluing nodes together can result in an arbitrary Ising spin network state. However, it may not always be the most optimal way to construct the network. For instance, gluing two open nodes together to form a dipole network would require 10 qubits instead of the 8 qubits needed for the basic method, which does not provide an advantage. However, in cases where a larger network has already been constructed using the open pentagram networks, adding a single node may prove to be advantageous.

To illustrate this, let us consider the hexagram network, which consists of 6 nodes. The construction scheme of the network is depicted in Fig. 20, where two nodes and four free links are involved.

The construction utilizes  $2 \cdot 5 + 4 \cdot 2 = 18$  qubits, which is a bit smaller than for the basic method, involving  $10 \cdot 2 = 20$  qubits. The corresponding 18-qubit quantum circuit is shown in Fig. 21.

It is important to note that to minimize the quantum resources needed to construct an arbitrary Ising spin network, one should consider the optimal combination of pre-existing open spin networks and free links. This requires careful consideration of the available resources and the desired network topology. However, determining the optimal sequence of gluing is a separate task that must be addressed individually, and depends on the specific details of the network being constructed. Finding the optimal strategy for constructing an Ising spin network with minimal quantum resources is an ongoing research challenge.

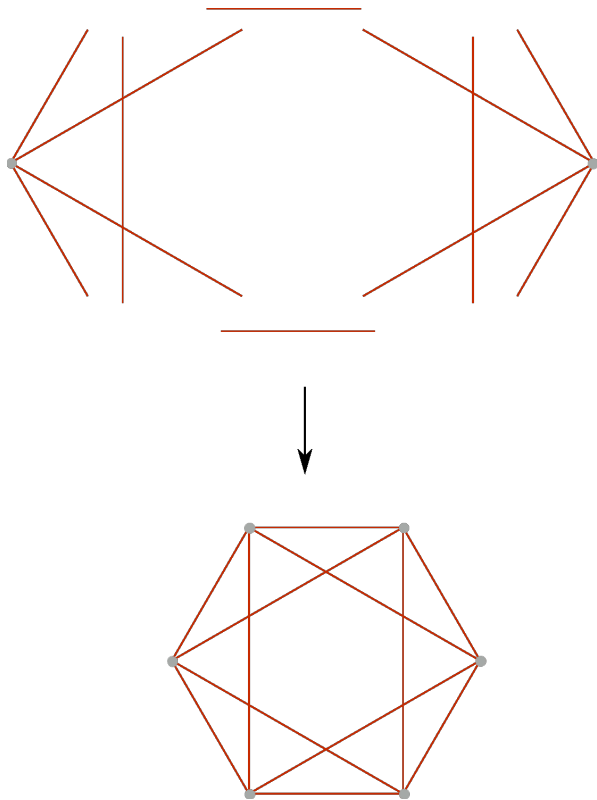


FIG. 20. Hexagram network obtained from two nodes each with four free links and from four additional links.

## VII. RESULTS

### A. Dipole

We employed the circuit illustrated in Fig. 9 to optimize a quantum device simulator, which was subject to statistical noise due to a finite number of shots, but not quantum noise. We used the PennyLane library for the simulations, which were run on an eight-qubit quantum device with 20,000 shots per circuit execution. To compute the gradient of the cost function, we utilized the parameter shift rule, while the classical Adam optimizer with a step size of 0.1 was chosen as the optimizer. Each optimization was halted after achieving convergence below  $10^{-6}$  or after 100 steps. Fig. 22 displays the history of the cost function for ten independent simulations with randomly initialized parameters.

After each minimization, we obtained the precise state described by the optimized parameter ansatz and calculated its fidelity with the expected theoretical state. Fig. 23 presents the mean fidelities and corresponding standard deviations obtained from ten independent simulations of the dipole.

### B. Pentagon

Here, we utilized the pentagram construction scheme illustrated in Fig. 24. The state corresponding to the open node utilized in the procedure was obtained using an exact simulator devoid of statistical noise. The simulations were executed on a 17-qubit quantum device simulator with 200,000 shots per circuit execution. To calculate the gradient of the cost function, we used the parameter shift rule, and we chose the classical Adam optimizer with a step size of 0.1 as the optimizer. Each minimization was terminated after achieving convergence below  $10^{-6}$  or after 100 steps. Fig. 25 displays the cost function's optimization history for ten independent simulations with randomly initialized parameters.

Fig. 26 shows the mean fidelities and standard deviations computed from ten independent simulations of the dipole problem.

### C. Hexagram

For this problem, we adopted the scheme depicted in Fig. 20. The state corresponding to the open node, which we employed in this procedure, was obtained using an exact simulator without statistical noise. The simulations were executed on a quantum device simulator with 18 qubits, and each circuit execution comprised 200,000 shots. To compute the cost function's gradient, we employed the parameter shift rule, while we chose the classical Adam optimizer with a step size of 0.1 as the optimizer. Each minimization was halted after achieving convergence below  $10^{-6}$  or after 100 steps. Fig. 27 presents the history of the cost function's optimization for ten independent simulations with randomly initialized parameters.

Fig. 28 illustrates the mean fidelities and corresponding standard deviations obtained from ten independent simulations of the hexagram problem.

### D. A 10-node graph

For this problem, we employed the scheme shown in Fig. 16. The state corresponding to the open pentagram, which we used in this procedure, was obtained using an exact simulator without statistical noise. The simulations were executed on a quantum device simulator with 16 qubits, and each circuit execution comprised 20,000 shots. To compute the cost function's gradient, we employed the parameter shift rule, and we used the classical Adam optimizer with a step size of 0.1 as the optimizer. Each minimization was halted after achieving convergence below  $10^{-6}$  or after 500 steps. Fig. 29 presents the history of the cost function's optimization for ten independent simulations with randomly initialized parameters.

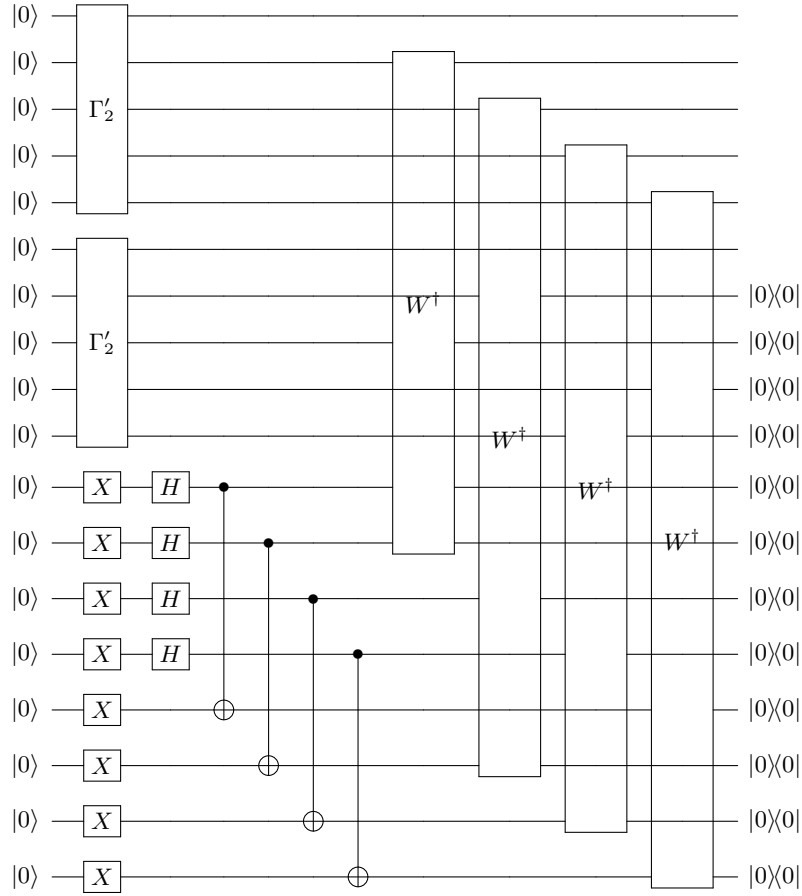


FIG. 21. Hexagram network obtained from two nodes, each with four free links ( $\Gamma'_2$ ) and from four additional links.

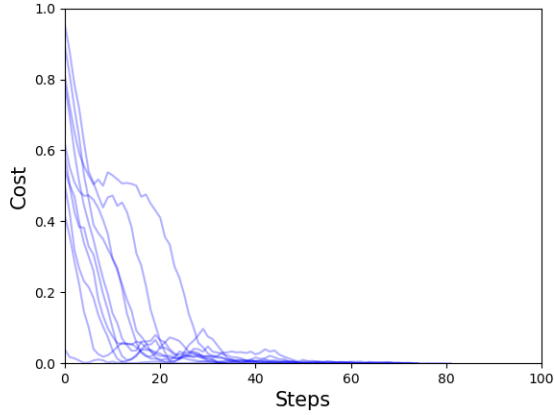


FIG. 22. The cost function for the dipole transfer with statistical noise for ten independent simulations with randomly initialized parameters.

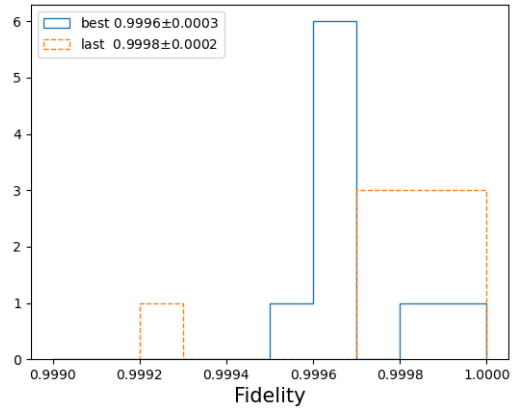


FIG. 23. Histogram of fidelities of dipole states obtained, at the last step (orange, dashed line), or at the step we the minimal cost value (blue, solid line).

## VIII. SUMMARY

Fig. 30 displays the mean fidelities and corresponding standard deviations obtained from ten independent simulations of the 10-node problem.

This article presents an optimized procedure for constructing quantum circuits that generate Ising spin net-

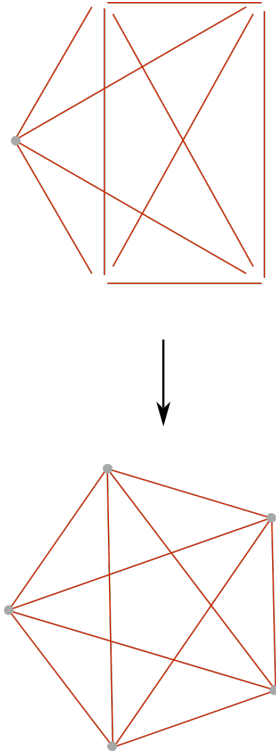


FIG. 24. Pentagram network obtained from a node with four free links and from six additional links.

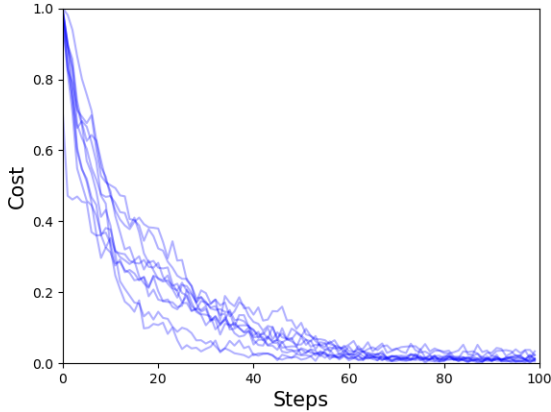


FIG. 25. The cost function for the pentagram transfer with statistical noise for ten independent simulations with randomly initialized parameters.

work states. These states are characterized by four-valent nodes with qubit degrees of freedom attached to them. Although other types of spin networks are more general, Ising spin network states are sufficient to model some important properties of quantum space, particularly with respect to the structure of quantum correlations, entanglement entropy, and the quantum thermodynamic limit.

The investigation was primarily motivated by the potential application of quantum computers in simulating

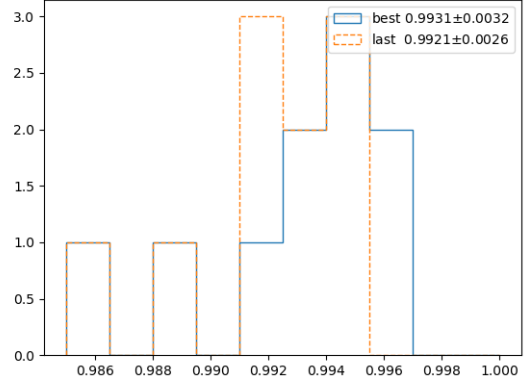


FIG. 26. Histogram of fidelities of pentagram states obtained, at the last step (orange, dashed line), or at the step we the minimal cost value (blue, solid line).

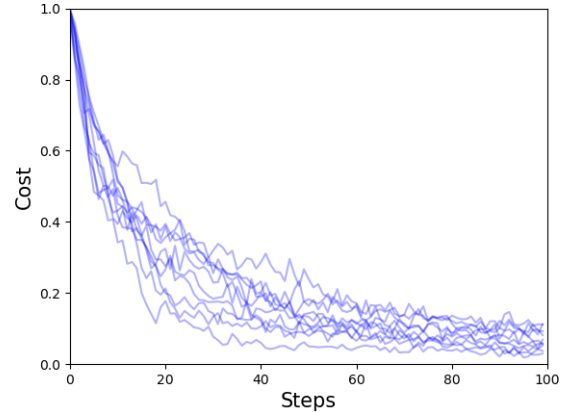


FIG. 27. The cost function for the hexagram transfer with statistical noise for ten independent simulations with randomly initialized parameters.

complex spin network states, which are currently beyond the capabilities of even the most powerful classical supercomputers. However, a key challenge in this field is the need to better understand the computational complexity of the relevant quantum amplitudes associated with spin network states. To determine the exact computational cost of such simulations, we must investigate the quantum circuit representation of these networks. By doing so, we can establish an upper constraint on the quantum complexity of these simulations and potentially even determine their exact value in certain cases.

An inefficient method for generating Ising spin network states involves using  $4n$  qubits to project link states and create a spin network with  $n$  nodes. In contrast, the method we introduce significantly reduces the number of required qubits, leading to practical benefits. Additionally, the introduced projection operator enables the

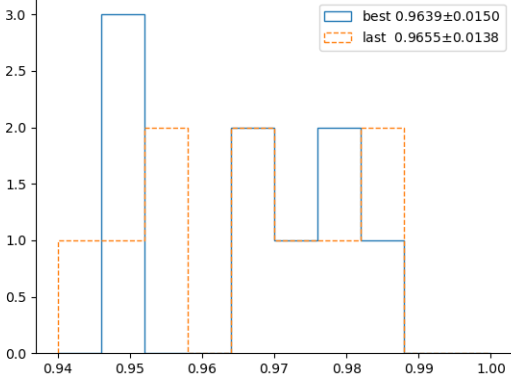


FIG. 28. Histogram of fidelities of hexagram states obtained, at the last step (orange, dashed line), or at the step we the minimal cost value (blue, solid line). In this case both lines overlap.

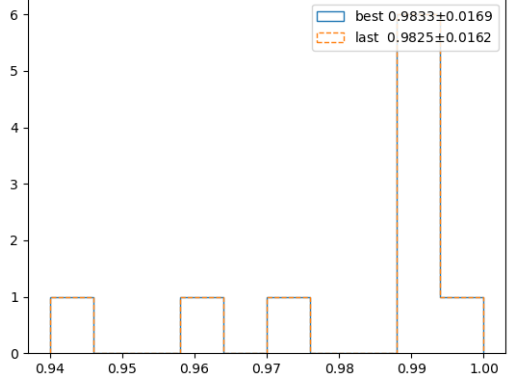


FIG. 30. Histogram of fidelities of 10-node spin network states obtained at the last step (orange, dashed line), or at the step we the minimal cost value (blue, solid line). In this case both lines overlap.

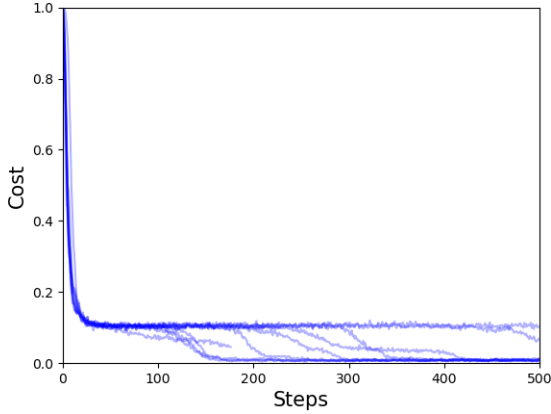


FIG. 29. The cost function for 10-node Ising spin network state transfer with statistical noise for ten independent simulations with randomly initialized parameters.

transfer of the final state onto an  $n$ -qubit ansatz circuit, allowing for further operations without the need for redundant qubits. This ansatz has numerous applications, including analyzing the quantum complexity of quantum-gravitational transition amplitudes and studying the fate of quantum fluctuations in geometric quantities and the scaling of quantum entropy. Our future studies will delve deeper into these topics.

In addition to the issues discussed so far, an important future direction of investigation is the study of partially projected states within the developed framework. In these states, the degrees of freedom at open links can be interpreted as boundary values, while the remaining network corresponds to the bulk. This approach has promising implications for understanding the possible holographic nature of gravitational interactions, and

can help address related problems.

Generalizations of the spin network state construction presented here to higher valence cases, beyond the Ising approximation, are also worth exploring. Additionally, future improvements in the methods of generating these states may benefit from utilizing the tensor network approach [17, 23].

**ACKNOWLEDGMENTS**

The research has been supported by the Sonata Bis Grant No. DEC-2017/26/E/ST2/00763 of the National Science Centre Poland. This research was funded by the Priority Research Area Digiworld under the program Excellence Initiative – Research University at the Jagiellonian University in Kraków.

**APPENDIX**

**Decomposition of  $\sqrt{SWAP}$  gate**

In Fig. 31 we present an explicit form of a circuit for the  $\sqrt{SWAP}$  gate, expressed in terms of the elementary single- and two-qubit gates.

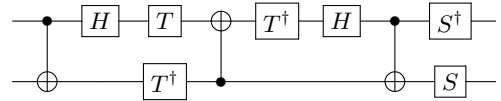


FIG. 31. Decomposition of  $\sqrt{SWAP}$  gate.

### Simplified circuit for the operator $\hat{W}$

Due to its complexity, applying operator  $\hat{W}$  (see Fig. 3) on current noisy quantum processors may lead to numerous errors. To overcome this issue, a simpler circuit that performs  $\hat{W}$  can be found using variational methods [24]. Fig. 32 illustrates the most intricate part of the circuit that needs to be simplified.

To simplify the circuit and reduce the likelihood of er-

rors on noisy quantum processors, we can substitute the intricate section with an ansatz circuit. By minimizing the cost function, we can determine the parameters that allow the new circuit to perform similarly to the operator  $\hat{W}$ , although it does not need to be an identical operator. The primary goal is to rotate one-qubit states into the intertwiner subspace of four qubits. The resulting circuit has the form depicted in Fig. VIII.

- 
- [1] C. Rovelli, “Loop quantum gravity,” *Living Rev. Rel.* **1** (1998), 1 [arXiv:gr-qc/9710008 [gr-qc]].
- [2] A. Ashtekar and J. Lewandowski, “Background independent quantum gravity: A Status report,” *Class. Quant. Grav.* **21** (2004), R53 [arXiv:gr-qc/0404018 [gr-qc]].
- [3] A. Feller and E. R. Livine, “Ising Spin Network States for Loop Quantum Gravity: a Toy Model for Phase Transitions,” *Class. Quant. Grav.* **33** (2016) no.6, 065005 [arXiv:1509.05297 [gr-qc]].
- [4] K. Li, Y. Li, M. Han, S. Lu, J. Zhou, D. Ruan, G. Long, Y. Wan, D. Lu and B. Zeng, *et al.* “Quantum Spacetime on a Quantum Simulator,” *Commun Phys* **2**, 122 (2019) [arXiv:1712.08711 [quant-ph]].
- [5] J. Mielczarek, “Prelude to Simulations of Loop Quantum Gravity on Adiabatic Quantum Computers,” *Front. Astron. Space Sci.* **8** (2021), 95 [arXiv:1801.06017 [gr-qc]].
- [6] J. Mielczarek, “Spin Foam Vertex Amplitudes on Quantum Computer - Preliminary Results,” *Universe* **5** (2019) no.8, 179 [arXiv:1810.07100 [gr-qc]].
- [7] G. Czelusta and J. Mielczarek, “Quantum simulations of a qubit of space,” *Phys. Rev. D* **103** (2021) no.4, 046001 [arXiv:2003.13124 [gr-qc]].
- [8] L. Cohen, A. J. Brady, Z. Huang, H. Liu, D. Qu, J. P. Dowling, and M. Han, “Efficient Simulation of Loop Quantum Gravity – A Scalable Linear-Optical Approach,” in *Frontiers in Optics / Laser Science*, B. Lee, C. Mazzali, K. Corwin, and R. Jason Jones, eds., OSA Technical Digest (Optical Society of America, 2020 [arXiv:2003.03414 [quant-ph]].
- [9] P. Donà, M. Fanizza, G. Sarno and S. Speziale, “Numerical study of the Lorentzian Engle-Pereira-Rovelli-Livine spin foam amplitude,” *Phys. Rev. D* **100** (2019) no.10, 106003 [arXiv:1903.12624 [gr-qc]].
- [10] P. Dona, M. Han and H. Liu, “Spinfoams and high performance computing,” [arXiv:2212.14396 [gr-qc]].
- [11] R. van der Meer, Z. Huang, M. C. Anguita, D. Qu, P. Hooijschuur, H. Liu, M. Han, J. J. Renema and L. Cohen, “Experimental Simulation of Loop Quantum Gravity on a Photonic Chip,” [arXiv:2207.00557 [quant-ph]].
- [12] P. Zhang, Z. Huang, C. Song, Q. Guo, Z. Song, H. Dong, Z. Wang, L. Hekang, M. Han and H. Wang, *et al.* “Observation of Two-Vertex Four-Dimensional Spin Foam Amplitudes with a 10-qubit Superconducting Quantum Processor,” [arXiv:2007.13682 [quant-ph]].
- [13] H. Ooguri, “Topological lattice models in four-dimensions,” *Mod. Phys. Lett. A* **7** (1992), 2799-2810 [arXiv:hep-th/9205090 [hep-th]].
- [14] J. W. Barrett, W. J. Fairbairn and F. Hellmann, “Quantum gravity asymptotics from the SU(2) 15j symbol,” *Int. J. Mod. Phys. A* **25** (2010), 2897-2916 [arXiv:0912.4907 [gr-qc]].
- [15] L. Freidel and S. Speziale, “Twisted geometries: A geometric parametrisation of SU(2) phase space,” *Phys. Rev. D* **82** (2010), 084040 [arXiv:1001.2748 [gr-qc]].
- [16] B. Baytaş, E. Bianchi and N. Yokomizo, “Gluing polyhedra with entanglement in loop quantum gravity,” *Phys. Rev. D* **98** (2018) no.2, 026001 [arXiv:1805.05856 [gr-qc]].
- [17] M. Han and L. Y. Hung, “Loop Quantum Gravity, Exact Holographic Mapping, and Holographic Entanglement Entropy,” *Phys. Rev. D* **95** (2017) no.2, 024011 [arXiv:1610.02134 [hep-th]].
- [18] A. Feller and E. R. Livine, “Entanglement entropy and correlations in loop quantum gravity,” *Class. Quant. Grav.* **35** (2018) no.4, 045009 [arXiv:1710.04473 [gr-qc]].
- [19] E. Bianchi, P. Donà and I. Vilensky, “Entanglement entropy of Bell-network states in loop quantum gravity: Analytical and numerical results,” *Phys. Rev. D* **99** (2019) no.8, 086013 [arXiv:1812.10996 [gr-qc]].
- [20] M. Cerezo, A. Sone, T. Volkoff, *et al.* “Cost function dependent barren plateaus in shallow parametrized quantum circuits.” *Nat Commun* **12**, 1791 (2021).
- [21] <https://github.com/Quantum-Cosmos-Lab/Ising-spin-networks>
- [22] E. Bianchi and E. R. Livine, “Loop Quantum Gravity and Quantum Information,” [arXiv:2302.05922 [gr-qc]].
- [23] E. Colafranceschi, G. Chirco and D. Oriti, “Holographic maps from quantum gravity states as tensor networks,” *Phys. Rev. D* **105** (2022) no.6, 066005 [arXiv:2105.06454 [hep-th]].
- [24] S. Khatri, *et al.* “Quantum-assisted quantum compiling.” *Quantum* **3** (2019): 140.

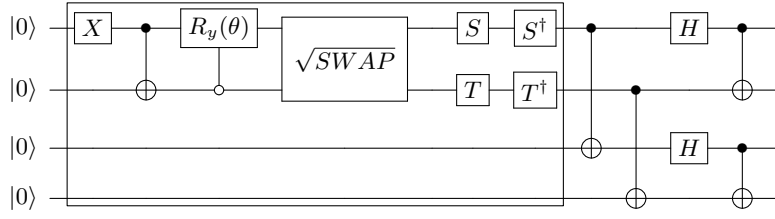


FIG. 32. Quantum circuit for the operator  $\hat{W}$  with the indication of the part being a subject of variational approximation.

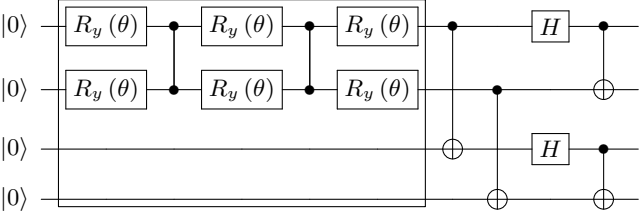


FIG. 33. Quantum circuit for the operator  $\hat{W}$  with the employed variational ansatz circuit.